Research Article Vol. 8, No. 2 / February 2021 / Optica 193

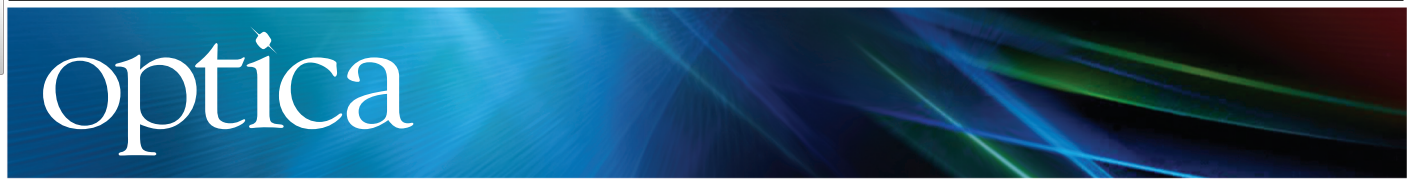

Networks of mutually coupled random lasers

Niccolò Caselli,[1,2,*] Antonio Consoli,[1,3,4] Ángel María Mateos Sánchez,[1] and Cefe López[1,5]

[1]Instituto de Ciencia de Materiales de Madrid (ICMM), Consejo Superior de Investigaciones Científicas (CSIC), Calle Sor Juana Inés de la Cruz, 3, 28049 Madrid, Spain
[2]Current address: Departamento de Química Física, Universidad Complutense de Madrid, Avenida Complutense, 28040 Madrid, Spain
[3]ETSI de Telecomunicación, Universidad Rey Juan Carlos, Calle Tulipán, 28933 Madrid, Spain
[4]e-mail: antonio.consoli@urjc.es
[5]e-mail: c.lopez@csic.es
*Corresponding author: ncaselli@ucm.es

Received 22 October 2020; revised 19 December 2020; accepted 29 December 2020 (Doc. ID 413223); published 8 February 2021

Random lasers (RLs) rely on light amplification in a gain material with feedback from multiple scattering in disordered media. They are unconventional light sources characterized by multiple narrow peaks emission with high potential in imaging and sensing applications. At variance with ordinary lasers, optical interaction between single RLs arranged in networks of multiply interconnected resonators remains unexplored. The typical RL architecture where gain material and scatterers are spatially mixed, is unsuitable for the realization of singular devices on the same platform. Here, we use RLs in which gain is restricted to the line between two scattering regions to establish and probe mutual coupling between many RLs. We prove the interaction in the network by detecting the spectral rearrangement of the compound emission as compared to individual RLs. The engineering of coupled RLs sets the basis for building structures with potential to function as optical neural networks.

https://doi.org/10.1364/OPTICA.413223

1. INTRODUCTION

Synchronization among coupled elements is a ubiquitous concept used for describing the dynamics of systems arranged in complex networks and in which non-linearity is an essential feature [1,2]. In order to engineer synchronization many architectures were proposed spanning from coupled oscillators [3,4] and mechanical modes [5], to fluid dynamics [6], synaptic neurons [7], or spatiotemporal chaos [8] in interacting lasers [9,10]. The basic requirement relies on the control of the collective interactions between the network elements. Among the possible optical implementations, nanophotonics has gained attention for mimicking both structural and functional features of neural networks by developing integrated optical circuits [11,12] where the non-linearity and chaotic behavior are given by the amplified light emission [13]. While synchronization has been largely tested in systems of interacting solid-state [10,14,15], fiber [16], and semiconductor lasers [17,18], pursuing the same effect in random laser (RL) architectures is emerging as a disruptive breakthrough due to the ease of fabrication that can give rise to complex networks [19–22]. At variance with equally spaced emission lines of Fabry–Perot lasers, emission spectra of RLs consist of narrow spikes randomly distributed in frequency [23]. RLs do not require the engineering of a high perfection cavity, since they are based on disordered media in which the feedback for lasing action is provided by strongly scattering elements [24,25]. Therefore, they demand easier manufacture, which allows inexpensive devices. The typical RL emission shows lower spatial coherence, furnishing speckle-free illumination [26], as well as enabling spectral super-resolution [27]. RLs and, more generally, optical random modes, have found application in a large variety of fields from energy harvesting [28], information processing [29], bright terahertz emitters [30] to sensing [31] and tumor cell recognition [32], to name a few. With potential to become a mature and accessible technology, these features furnish an additional spectral dimension to the non-linearity, which enriches the interaction and provides opportunities to unveil fundamental physics, since RLs can act as elements of optical network architectures.

To date no experimental studies have analyzed the optical interaction between independent resonators in networks of RLs. The most widespread RL implementation is currently based on distributed feedback where the scattering centers are randomly placed inside the optically active medium [23,33]. Its spectral signature is unique to the spatial distribution of scattering centers, given the shape of the pump.

We previously introduced an alternative configuration with non-distributed feedback, in which the region of gain medium being pumped is restricted to a strip joining two (passive) scattering volumes [34] or surfaces [35], providing both feedback and output coupling. This structure recalls a Fabry Perot implementation in which flat mirrors have been substituted for scattering materials. Nevertheless, no periodic spectrum is expected—or observed—and the same random distribution of frequency peaks is extracted

from both laser ends, where scatters with different shape and spatial distributions are placed. In our implementation, a resonator is comprised of a narrow stripe pumped region and two air holes exhibiting rough surfaces. The holes act as mirrors with embedded disorder and therefore can provide feedback necessary to sustain RL behavior [36]. These RLs show stationary emission spectra, since the geometry of such configuration remains static, thus allowing coupling between modes in a single RL to be studied [37].

In this paper, we demonstrate that modal interaction can be induced in multiple disordered resonators, giving rise to a new class of active optical networks based on interconnected and coupled RLs. The network, defined in the plane of the gain material, is determined by several, distant, scattering centers (air holes with disordered sidewalls) multiply connected by pumped stripes. The system can be considered as a single, collective resonator in which manifold coupled oscillators are turned on at will (by turning on the corresponding pumping stripe). This is proved by the fact that highly correlated spectra are observed at all the nodes of the network.

Simple numerical calculations based on coupled mode theory were carried out and predictions on the spectral redistribution induced by the interacting RL network were found in qualitative agreement with the observed behaviors. Finally, since a single network node can be used as scattering and coupling element shared between many resonators, more complex network architectures can be envisioned as "*join-the-dots*" graphs in order to extend the proposed approach.

2. EXPERIMENTAL SETUP

A. Sample Preparation

The typical single RL we used, representing the building block of RL networks, is composed of two distant (≈ 2 mm) disordered scattering centers acting as rough mirrors and connected by a laser pumped stripe. The active medium in which the random lasing occurs is a solid, dye-doped biopolymer thin film in which the polymer matrix has been chosen for its ability to prevent dye quenching [38,39]. The films were produced by introducing 4-(dicyanomethylene)-2-methyl-6-(4-dimethylaminostyryl)-4H-pyran (DCM), with a 0.35% mass concentration in a deoxyribonucleic acid (DNA)-cetyltrimethyl ammonium (CTMA) polymer matrix. The cationic surfactant CTMA (Sigma-Aldrich 292737) was used to make the DNA (Sigma-Aldrich D1626) soluble in organic solvents and then easily miscible with the DCM dye solution. The DNA-CTMA complex was dissolved (4 vol. %) in ethanol and mixed with the DCM solution (0.5 vol. % in equal parts of ethanol and chloroform). The resulting blend was magnetically stirred for 5 h. Then it was spread by dropcasting onto a glass substrate, and solid films with a thickness of about 20 μm were obtained after drying the sample at room temperature and pressure.

B. Scattering Elements

The networks of RLs are realized by inscribing scattering centers by means of a direct laser-writing technique into the polymer film and then by optically pumping the dye–polymer region through an ensemble of stripes projected on the sample surface [see the schematics of Fig. 1(a), the out-of-plane emission shown in Fig. 1(b)]. In order to fabricate the scattering centers the polymer was locally ablated by a short-pulsed (100 fs), high-energy (∼250 μJ/pulse) Ti:sapphire laser emitting at 800 nm peak wavelength. The laser power, the number of shots delivered, and the focusing position were controlled by using a half-wave plate in conjunction with a linear polarizer, a software controlling the laser output, and motorized translational stages, respectively. A single laser shot focused by a lens of 5 cm focal length drilled a hole in the polymer matrix. To create a reproducible hole size, we overcame the shot-to-shot laser power fluctuations by lowering the power and increasing the number of pulses (50 single shots) delivered to obtain each hole. This assured that, in the energy range between 200 and 300 μJ/pulse, the local ablation removed completely the polymer and reached the underlying glass substrate, thus leaving a cylindrical-like air defect in the polymer matrix. By varying the laser fluence we achieved reproducible holes with a diameter size that can be varied in the range 30–150 μm. Each scattering center consists of a single [Figs. 1(d) and 1(e)] or a series of holes (diameter of tens of micrometers), as those reported in Figs. 1(b) and 1(c). The hexagonal pattern arrangement obeys only practical reasons and no advantage is derived from their regularity beyond the economy of manufacture. The rough internal surfaces of each drilled hole form a disordered air/polymer interface whose mission is to strongly scatter light coming from the pumped volume [see Fig. 1(b)], thus providing random feedback for lasing action. The number of laser modes sustained by a RL with non-distributed feedback, as well as their threshold, has been proven to depend on the roughness and porosity of the scattering surfaces [35,40].

C. Random Lasers Measurements

The excitation setup involves a 10 ns pulsed, frequency-doubled 532 nm Nd:YAG laser with a 10 Hz repetition rate, whose beam was shaped by an amplitude spatial light modulator working in reflection, which allowed changing the pumping scheme on the sample with no moving parts. By means of this scheme we imaged on the sample surface the intensity distribution required to produce the desired optical pumping geometry. We drew a set of stripes of the same length (2 mm) and width (50–100 μm) connecting scattering centers, as reported in Figs. 1(a) and 1(b). The out-of-plane lasing emission was imaged, with a magnification equal to 2, both on a CCD, see Fig. 1(b), and on a plane where the tip of an optical fiber collected the signal, which was coupled to a spectrometer and a detector (SPEC, Andor Shamrock 303). We achieved a spatial and spectral resolution of 50 μm and 0.1 nm, respectively. The fiber tip was mounted on motorized translation stages in order to collect the radiation emerging from different scattering centers. Therefore, lasing emission was detected orthogonally to the sample surface, at node positions where lasing light is scattered out of the plane by the scattering centers. As previously mentioned, random modes in this kind of RL emerged as stable (for about 10^4 successive acquisitions) sub-nanometer wide spectral peaks and the same resonances are recorded at both ends (see Figs. S1 and S2 of Supplement 1). This confirmed that the device consisting of a pumping line and two scattering centers was acting as a single oscillator with its unique spectral signature [34]. It is important to stress that by applying this pumping scheme, and by triggering the spectral acquisition with the laser repetition rate, consecutive spectra are independent from one another, since they refer to different excitation pulses. In order to prove the stability

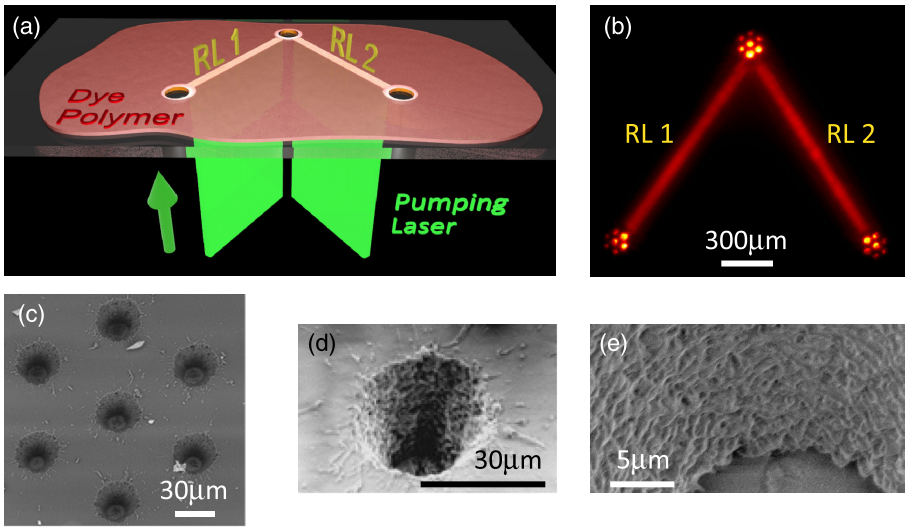

Fig. 1. RL network fabrication. (a) Schematics of the RLs network. The dye-doped polymer thin film is deposited on a glass substrate and disordered scattering centers are created by drilling the film. Optical excitation is performed by a spatial light modulator sculpted laser impinging from the bottom and uniformly pumping regions that connect the scatterers. (b) Emission intensity image (acquired by CCD) of two RLs pumped simultaneously. Each resonator consists of a rectangular pumped volume placed between two scattering centers each made of seven holes with disordered internal surfaces. (c)–(e) Scanning electron microscopy (SEM) images of one of the scattering centers in (b), reported with increasing magnification to highlight, inside a given hole, the rough sidewalls, which are responsible for the RL feedback action.

during the entire acquisition time, we repeated a sequence of illumination frames, each of which contains a different pumping lines configuration in the network. For instance, referring to Fig. 1(b) the sequence was composed by three frames containing line 1, line 2, both lines 1 and 2, respectively. For each frame we acquired 50 consecutive spectra, corresponding to 50 laser single shots, to be averaged. The sequence was repeated many times. Therefore, for each illumination geometry we achieved a series of nominally identical spectra mixed in time. In every series the spectral fluctuations were minimal, exhibiting a high degree of correlation (see Fig. S2, Supplement 1) over a period of about 5 min. After longer times of constant exposure above laser threshold, the polymer matrix suffered modifications due to the induced heating, hence causing the spectrum to slowly change and to experience a correlation decrease with respect to the initial one that usually led to a complete decorrelation after 15 min. On grounds of such stability analysis, for every investigated RL configuration we performed a series of 10 nominally identical acquisitions, averaged to obtain a reliable spectral signature. More details concerning pumping threshold, integration time, and stability can be found in Supplement 1.

3. RESULTS AND DISCUSSION

A. Coupling in a Network

For the sake of simplicity, before extending the study to more complex geometries, we demonstrate the functionality by focusing on the basic building block of a network: two equivalent RLs connected through a node. In this configuration, we prove that the emission from one RL can be affected by the action of the second RL with which it has a scattering center in common. Then we will prove RL interactions in ring networks of three resonators.

When considering RL networks, one must establish a protocol to determine if oscillators are interacting with each other. A simple approach is to compare the sum of the spectra obtained from single resonators (turned on one at time) with the emission detected when all resonators are simultaneously active. If no interaction occurs, a high degree of correlation will emerge from the comparison, as the emission of the whole network will be the linear sum of each oscillator contribution. On the contrary, if coupling between different oscillators is taking place, the compared spectra will be different since the network emission will be a non-linear mix of the single contributions.

Two different RLs provide spectra that can be taken as standard for independence (negligible correlation) whereas two spectra taken successively from a single RL (only subject to stochastic fluctuations) can be used as standard for strong dependence and similarity, since high correlation is assured.

We started by addressing the simplest case consisting of two RLs having one scattering node in common. In this configuration, two resonators activated one at a time show distinct, uncorrelated spectra that we take as the benchmark of spectral independence. When both RLs are pumped simultaneously, if they do interact the emerging spectral features must depend on the lasing state of both resonators. Several circumstances can be expected to occur such as frequencies common to both uncoupled resonators not belonging to the compound one, modes from some resonator becoming available to the compound one, modes not lasing in any resonator showing as a consequence of the coupling and, generally, changes in mode gain. The fingerprint of an effective interaction would thus be a spectral modification, i.e., peak wavelength shifts and/or an intensity redistribution, that may be detected at every network node. With this in mind, we tested coupling between two different RLs by acquiring spectra of each single laser and comparing their sum to the spectrum emerging from the simultaneous activation of both RLs in the network. To set a standard for uncoupled RLs we first studied the device reported in Fig. 2(a), where two RLs (labeled 1 and 2) share the scattering center B. The device is composed by three scattering nodes made of single holes connected by two pumping lines. The two single RL emissions are expected to be independent, as they originate from two different resonators

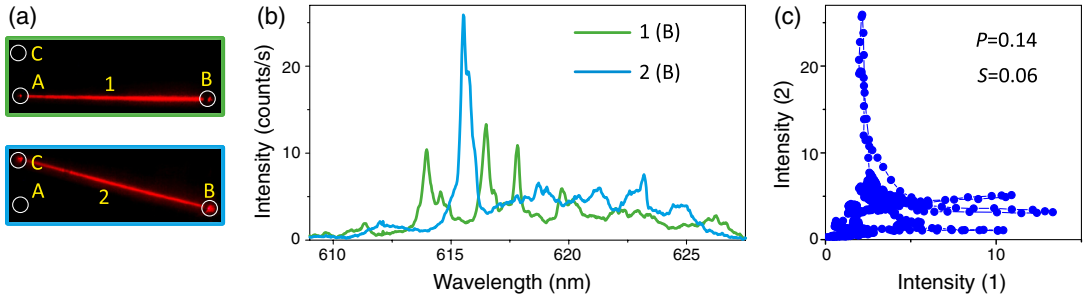

Fig. 2. Two independent RLs with scattering centers made of single holes (30 μm diameter size) with disordered surface, as an example of fully uncorrelated spectra. (a) Out-of-plane emission maps of RLs 1 and 2, obtained by pumping line 1 and 2 (length 2 mm), which connect the scattering centers A–B and B–C (highlighted inside white circles), respectively. (b) Spectrum of RL 1 (green curve) and of RL 2 (cyan curve) both acquired at position B. (c) Parametric plot of the intensity of the spectra in (b). The values of the Pearson correlation (P) and of the area of the parametric plot (S) are reported.

non-simultaneously activated and, as shown in Fig. 2(b), their spectra show two uncorrelated sets of peaks.

In order to visually highlight the low correlation and spectral difference between the two RLs, in Fig. 2(c) we reported the intensity of the first spectrum as a function of the intensity of the second one, for every acquired wavelength: each data point having coordinates $[I_1(\lambda_i),\ I_2(\lambda_i)]$ for $i = 1 \ldots n$, with n corresponding to the number of wavelength data. This representation will be hereafter called parametric plot. Since in this picture the vast majority of data lay outside the diagonal line, a low linear correlation is evident, as quantified by the small value of the Pearson coefficient being $P = 0.14$ [41,42]. The non-zero value of P can be attributed to the contribution of emission background. Fully correlated spectra from the same RL are shown in Fig. S2 of Supplement 1 ($P > 0.97$). The high intensity peaks of one RL lying on background intensity regions in the other RL appear as vertical and horizontal streaks, while data in fluorescence background regions of both resonators appear as a cloud at lower intensities. Obviously two proportional spectra would give a straight line in this kind of representation, with the Pearson correlation directly proportional to the regression coefficient.

An additional measure to assess the degree of similarity between spectra, can be provided by the surface area (S) enclosed by the lines that connect the parametric plot data. The surface area measure increases with shifted, overlapping peaks but, at variance with Pearson's correlation, it attains very small values both for high correlation (e.g., between nearly proportional spectra; see Figs. S3 and S4 of Supplement 1) and low correlation [vertical and horizontal streaks in Fig. 2(c)]. Therefore, a high S value implies that the overlap is not complete, but that the spectra exhibit small variations in the peak positions and/or amplitudes, as occurs if an effective weak interaction was in place. In our analysis, it is the conjunction of the parameters P and S that allows estimation of the coupling between single RLs in the network. For instance, for the two independent RLs reported in Fig. 2 the low value of both parameters ($P = 0.14$ and $S = 0.06$) proves the negligible correlation between them.

When two resonators do couple, this interaction must appear as a difference between the sum of their independent spectra and the compound spectrum obtained with simultaneous pumping. We took the dissimilarity between these spectra as a smoking gun of coupling. For the RLs introduced in Fig. 2 we proved this dissimilarity by simultaneously pumping both lines; see Fig. 3(a). When both RLs are active, the compound spectrum (1&2), reported in Fig. 3(b) (red line), was acquired at the common scattering node, in order to overcome fluctuations in the out-of-plane emission between different nodes. This emission was compared to the sum of the separate spectra taken successively (1 + 2) at the same node, reported in Fig. 3(b) (blue line). If no interaction were taking place, each RL would independently scatter their emission out of the network and the compound emission would be the sum of the two single RL spectra, resulting in strong overlap and high correlation ($P \approx 1; S \approx 0$). The extreme opposite would lead to the compound spectrum retaining no features from either resonator, thus bearing no resemblance with their sum, in which case a streaked parametric plot would result ($P \approx 0 \approx S$). A case where $P \approx 0$; $S \approx 1$ cannot occur for spiked spectra (or even background fluorescence) as it is a signature of fully random noise signal.

In Figs. 3(b) and 3(c) the sum spectrum shows a clear difference with the emission detected from the compound resonator, exhibiting lessened correlation, $P \approx 0.87$, and a moderate area $S \approx 0.23$. Typical values for correlation in successive acquisitions of one resonator emission (see Fig. S2, Supplement 1) provide a benchmark for highly correlated spectra as high as $P \approx 0.98$. A redistribution of the spectral density with suppression and/or enhancement of existing modes, up to the occurrence of new ones, is observed. It is remarkable how the compound emission is dominated by two strongly enhanced peaks at 615.6 nm (giving rise to the large loop in the parametric plot, responsible for most of the value of S) and 619.7 nm (originating one large vertical streak), while the majority of the emission is inhibited with respect to the sum spectrum. The emission stability of the RLs was checked in every spectral acquisition (see Fig. S2, Supplement 1) and the differences observed between the sum and the compound spectra cannot be ascribed to variations in the exciting conditions, polymer degradation, or detection instabilities.

Investigation of 20 network devices with the same design revealed that the spectral rearrangement occurs with large variations, as depicted in Fig. S5 of Supplement 1. We found fingerprint of coupling ($S > 0.15$ and $P < 0.9$) in 40% of the cases. This inhomogeneity is the result of random variations in mode gain and coupling strength, which depends on the specific features of the resonators and on spectral and spatial overlap of RL modes, that cannot be engineered *a priori*. The analysis presented in this work aims to prove that individual RLs composing a network can exhibit mode coupling between them.

Apart from investigating the sum versus compound spectral similarity at the common node, another experimental approach worth studying to prove mode coupling is evaluating how one RL emission from nodes that are not shared is influenced by the network interaction. Moreover, to prove the universality of the

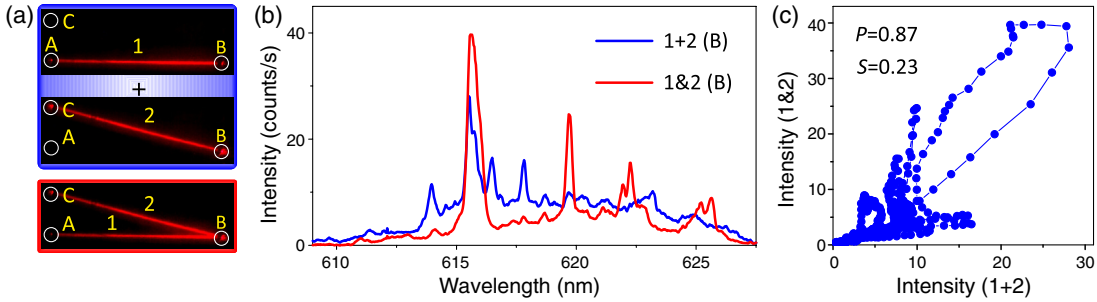

Fig. 3. Network of RLs made of the two devices reported in Fig. 2. (a) Out-of-plane emission of the RL network achieved by the simultaneous pumping of RLs 1 and 2 (red box) compared to the single RL emissions (blue box). (b) Spectrum of the RL network (1&2, red curve) and spectrum obtained by summing the single RL emissions (1 + 2, blue curve), detected in position B. (b) Parametric plot of the intensity of the spectra reported in (a). The values of Pearson correlation (P) and of the area of the parametric plot (S) are reported.

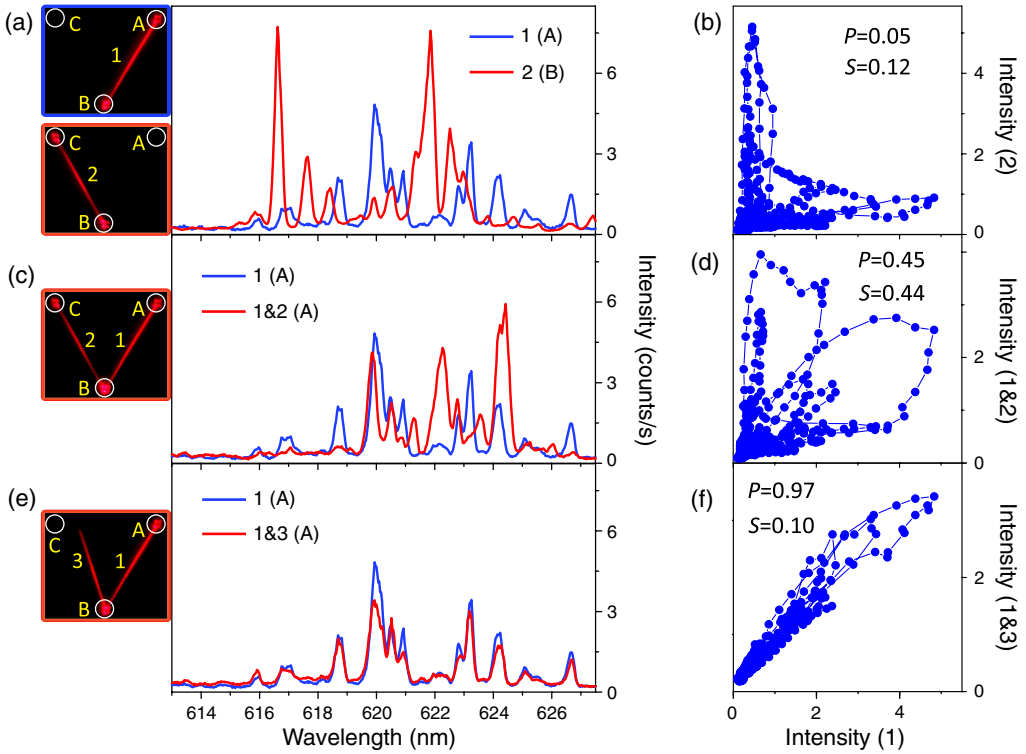

Fig. 4. RL network with three scattering centers made of four holes with disordered surface. (a), (b) Emission map, spectrum, and parametric plot of two independent RLs. The spectrum of RL 1 was acquired in position A (blue curve) while the spectrum of RL 2 in position B (red curve). The low correlation between the two is proved by the low values of P and S. (c), (d) Network formed by RLs 1 and 2 simultaneously active. The network spectrum (red curve, acquired in A) is compared to the spectrum of RL 1 reported in (a) and exhibits strong variation highlighted by the values of P and S. (e), (f) No interaction was observed between RL 1 and pumping line 3 that does not connect two scattering centers, thus it is not a RL. No significant variations are induced in the spectrum collected in A, which exhibits strong correlation with RL 1 alone.

coupling occurrence, we varied the geometry of the scattering centers by fabricating networks with three nodes positioned at the corners of an equilateral triangle, each consisting of four holes arranged in a square pattern, as reported in Fig. 4. Two single RLs are established by pumping the lines that connect corners A–B (line 1) and B–C (line 2), respectively, as shown in Fig. 4(a). The corresponding parametric plot, Fig. 4(b), demonstrates the low correlation between spectra from two independent single resonators ($P = 0.05; S = 0.12$). To test the influence of RL 2 on the emission of RL 1, spectra were collected at position A when RL 2 was [Fig. 4(c) red line] or was not pumped [Fig. 4(c) blue line]. In this position the emission of RL 2 alone is null in the absence of RL 1 action (see Fig. S6, Supplement 1), so that, trivially, the sum 1 + 2 equals the emission of RL 1. When RL 2 was turned on, new modes got amplified through line 1 and were observed in node A, for instance those at 608 and 623 nm, which belong to the emission of RL 2. At the same time, some modes experienced a suppression, such as those at 614 and 616 nm. The parametric plot, reported in Fig. 4(d), furnishes a heavily reduced linear correlation, $P = 0.45$, and a high area value, $S = 0.44$, thus bearing evidence of an interaction between the two RLs.

In order to close down the definition of coupled RLs network, we study in Figs. 4(e)–4(f) the impact on a single RL of a pumping stripe that does not connect two scattering centers (i.e., not a RL) or lines that intersect the said RL (see Figs. S7 and S8 of Supplement 1). These cases do not show spectral redistributions,

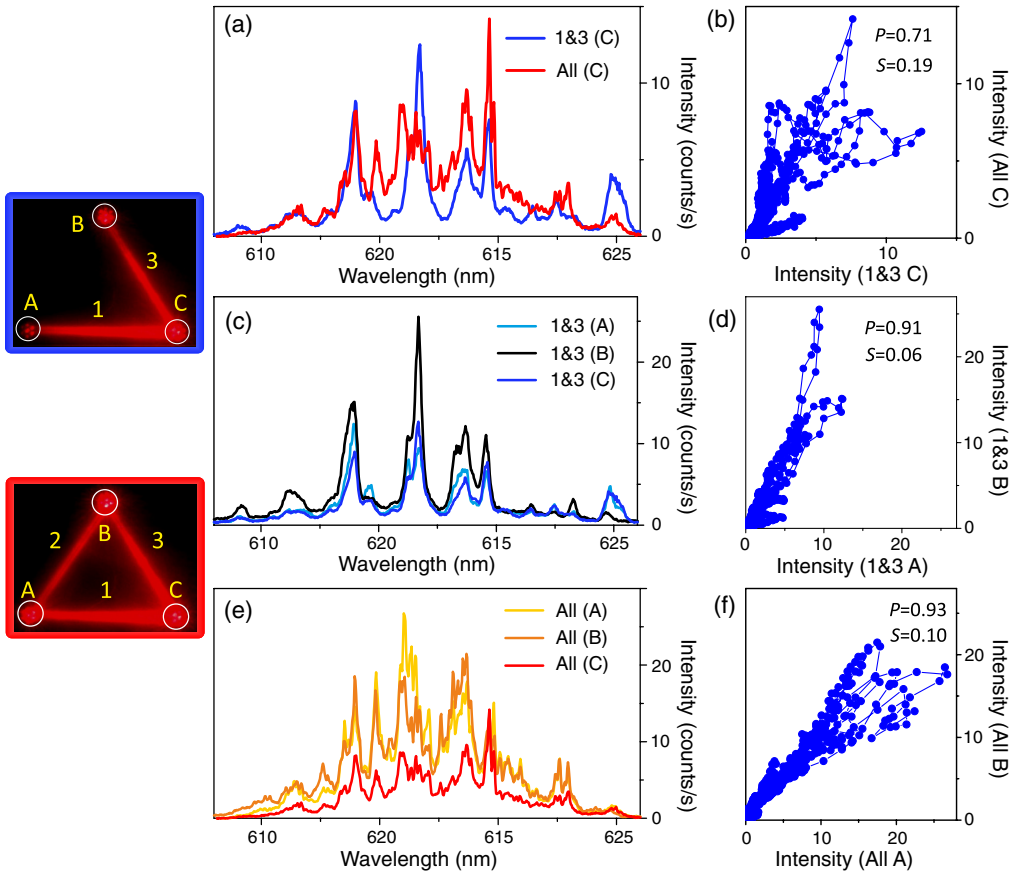

Fig. 5. Ring RL network with three scattering centers made of holes with disordered surface and arranged in hexagonal pattern. (a), (b) Spectrum and parametric plot, respectively, obtained by pumping RLs 1 and 3 simultaneously (blue curve), and by pumping all three lines at the same time (red curve). The influence of RL 2 at position C is proven by the spectral redistribution quantified by $P = 0.71$ and $S = 0.19$. (c), (d) Spectra collected at every node position (A, B, and C) when RLs 1 and 3 are simultaneously active and parametric plot comparing the spectra acquired in A and B (nodes not directly connected). The high correlation between them proves the establishment of a single large RL resonator. (e), (f) Global network spectra acquired at every node and parametric plot comparing the total emission in A and B, showing high correlation. Further parametric plots of the spectra in (c) and (e) are reported in Fig. S9 of Supplement 1.

thus precluding the inclusion in a coupled network. This finding highlights the requirement to share a scattering node for a RL to belong to the network. Further examples are reported in Fig. S6 of Supplement 1. Additionally, the fact that simply crossing does not make RLs link into a network, eases the design and augments the possibilities in 2D network building.

B. Ring Network

A ring RL network, still simple yet more complex than the one investigated in Fig. 4, was considered too. It consists of three disordered scattering nodes each made of seven holes with rough internal surface [see Figs. 1(b)–1(e)] that can be joined by three pumping stripes. Here, we exploited all three single RLs emerging by pumping the device with stripes connecting the scattering centers. We focused on the effect induced by switching on/off a single RL of the network. The strong variation of the network emission induced by turning on/off the pumping line A–B (RL 2) and extracted from C (that does not belong to RL 2) is reported in Figs. 5(a) and 5(b). The parametric plot of the spectra collected when (i) only lines 1 and 3 are pumped and (ii) the three lines are active at the same time, gives $P = 0.71$ and $S = 0.19$, indicating a strong spectral modification that, again, produces a reduced correlation. In this case the coupling fingerprints are the spikiness of the spectra causing small wavelength shifts and large intensity variations, which contribute to large loops in the parametric plot. A similar behavior was found at the other nodes (in A $P = 0.70$, $S = 0.17$ and in B $P = 0.67$, $S = 0.22$) when changing the two pumping lines, as reported in Fig. S9 of Supplement 1.

In Figs. 5(c)–5(f) we report the spectra acquired at every node position when only RLs 1 and 3 are turned on and when the entire network is active. Although intensity variation is present, remarkably, the peak positions remained almost unchanged. The parametric plots that compare the spectra one-on-one, prove the high correlation among all of them ($P > 0.9$ and $S < 0.1$). The remaining parametric plots are reported in Fig. S9 of Supplement 1. The observed intensity fluctuations are associated with the scattering efficiency of the "mirrors" that couple out the same mode differently, thus giving rise to spectra with intensity variation but still exhibiting high correlation. This demonstrates that the same modes are detected at the three network nodes, proving that the system behaves much like a single, compound resonator with modes that cannot be exclusively associated with a given RL.

Comparison between the three scattering centers morphologies presented in this work shows that larger hole number, i.e., increased

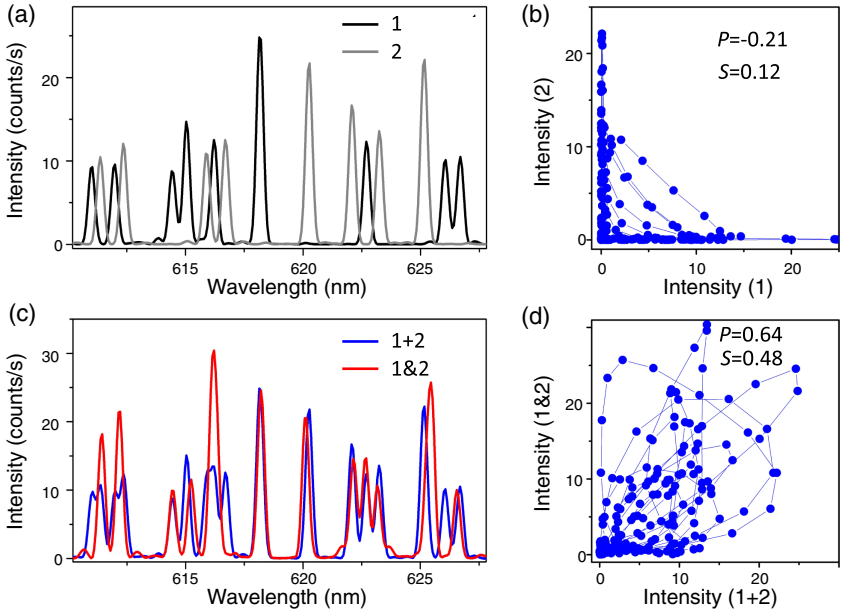

Fig. 6. Numerical simulation employing coupled mode theory. (a), (b) Spectra corresponding to two independent RLs, black and gray curves in (a), show a low correlation in the parametric plot in (b). (c), (d) The sum of the spectra in (a) (1 + 2, blue line) is compared to the compound spectrum (1&2, red line) obtained by introducing a coupling term between the two sets of modes. The coupling gives rise to an intermediate value of Pearson correlation ($P = 0.64$) and a high area parameter ($S = 0.48$), which therefore can be used as experimental evidence of RLs interaction.

disorder surfaces, boosts the chances to establish coupling. The analysis based on the conjunction of the Pearson's correlation and the enclosed area allowed estimation of the spectra (di)similarity, thus bearing information on the RL network coupling, since it induces a spectral redistribution of the amplified modes. With respect to other methods that evaluate the similarity between different spectra, such as the autocorrelation function [43] or the mutual information [44], our method gives a remarkable outcome in highlighting spectral redistributions (see Fig. S10, Supplement 1).

C. Numerical Model

We simulated the RLs network in the framework of time coupled mode theory [45,46]. For each resonator, the temporal and spectral evolution of each of its modes were considered (no spatial information was included). We introduced mode gain, losses, coupling, and gain saturation, while, for the sake of simplicity, we neglected other second-order non-linear effects. The system under investigation was numerically replicated by a set of $N = 40$ random possible lasing frequencies, almost evenly spaced (a 5% degree of fluctuation from equispaced was added) in order to cover the spectral range of interest. In order to simulate the experimental lasing spectra, we considered that in each single RL 10 different modes ($j, k = 1 \dots 10$, randomly selected among the N globally defined) were allowed to exist. All modes satisfied the following time-dependent set of differential equations:

$$\dot{a_k} = i\omega_k a_k - \alpha_k a_k + \sum_{j \neq k} c_{j,k} a_j + g(t, \omega_k) \frac{a_k}{1 + \gamma_k |a_k|^2}, \quad (1)$$

where $a_k(t)$ is the complex amplitude of the kth mode as a function of time, ω_k is its frequency, α_k are the losses, $c_{j,k} \propto |\omega_k - \omega_j|$ is the coupling coefficient with all other jth modes that fades with frequency separation, $g(t, \omega_k)$ is the time-dependent mode gain (pump pulse), and γ_k is the gain saturation coefficient, considered equal for all modes. Equation (1) describes how the kth mode evolves in time. By Fourier transforming the solution, we obtained the spectral profile in amplitude and phase of each mode and the full RL spectrum was retrieved by summing the intensity of all modes. The excitation pulse was designed to reproduce the pump used in experiments with about 10 ns and a gain bandwidth of about 30 nm. The maximum value of the coupling was chosen as $c_{\max} = 1.5 \cdot 10^{-5}(g_{\max} - \alpha_{\max})$. The same coupling matrix was used for calculating the spectra of the single resonators and of the coupled compound where all the modes interact simultaneously. The introduction of mode coupling implies that the instantaneous frequency of the kth mode, defined as the time derivative of the phase, varies with respect to its initial value, ω_k as a function of time, depending on the coupling to other modes. This effect explains the frequency shift from ω_k, so that adjacent modes can partially overlap until, in the limit of high coupling, a single peak emission was found. In the framework of coupled mode theory, the peak modification is due to energy exchange in time between interacting modes.

In this way, two independent RLs are represented by two sets of 10 modes randomly chosen from the pool, for which Eq. (1) was solved separately, that is, couplings are only considered within the 10-sets giving rise to the gray and black spectra reported in Fig. 6(a), respectively. Notice that, due to the coupling, not all modes necessarily show up in the spectrum, having merged with neighboring ones. The parametric plot of Fig. 6(b), heavily dominated by vertical and horizontal streaks, highlights the very low correlation between them.

In modeling the case of two coupled RLs, Eq. (1) was solved considering that the two 10-sets of modes owned by each RL contributed in the equation, as they were pumped at the same time. The resulting compound spectrum, 1&2 [red line in Fig. 6(c)], was compared to the sum of the single resonators, 1 + 2 [blue line

in Fig. 6(c)]. The coupling gave rise to a spectral redistribution with respect to the sum of the stand-alone emissions. In fact, the frequency and intensity of the peaks are slightly changed, with attraction/repulsion between adjacent modes and energy transfer due to the mode interaction. The corresponding parametric plot of Fig. 6(d) resembles the experimental observations reported in Figs. 3(c), 4(d), and 5(b) by showing a linear correlation $P = 0.64$ along with a high area parameter $S = 0.48$. This demonstrates that in the presence of an effective interaction, the spectra show a reduced linear correlation along with a high area value, as we found experimentally. By averaging the results of 20 simulations that compare (1 + 2) to (1&2) with different sets of independent modes and coupling strength, we found consistent behaviors (see Fig. S11 of Supplement 1), proving that this simple model was able to grasp the relevant insight about the coupling in a network of RLs.

4. CONCLUSIONS

We realized multiple RLs in a planar morphology by inscribing disordered scattering nodes in a film of gain material made of dye-doped biopolymer and selectively pumping the stripes joining them. The drilled holes acted as scattering elements, with rough surface between polymer and air, that were able to backscatter radiation into the pumped stripe and, at the same time, to forward scatter light thus establishing mutual interaction with any resonators sharing the same scattering node. By designing networks of such RLs, we proved that it is possible to induce an effective coupling between them. Spatially resolved probing and spectral correlation analysis allowed us to detect their synchronous ensemble interaction. Tests of different configurations consistently show the network coupling when RL resonators are fully formed (pumped stripe joining two end scatters) and the linking includes them in the network (at least one of the nodes is shared). Our findings are supported by time coupled mode theory calculations that predicted the spectral correlations, giving a qualitative account of the observed behavior.

The presented architecture has a small footprint, low fabrication complexity and cost, ample possibilities for multiple connectivity, and is intrinsically non-linear making it a good candidate to study highly non-linear interactions in networks. Spatially modulated pumping, where different RLs in the network can be selectively pumped with different pulse energy sent with selected timing to each of them, enables a versatile random network platform. Additionally, since the RLs spectral responses are sets of $I(\lambda_i)$ and not simple one-bit states, the exchanged signals present a vectorial character that, together with the fact that each node can be independently probed, further increases the dimensionality of the system. We believe that all the reasons above will trigger the study of more complex networks based on RLs, possibly paving the way to realize photonic neural network architectures.

Funding. Ministerio de Ciencia e Innovación (project RTI2018-093921-B-C41).

Acknowledgment. Álvaro Blanco and Francesco Riboli are thankfully recognized for fruitful discussions. N. C. acknowledges MCIU *Juan de la Cierva* program.

Disclosures. The authors declare no conflicts of interest.

Data Availability. The data that support the plots within this paper are available from the corresponding authors upon reasonable request. The MATLAB codes developed to execute the calculations presented in this paper are available from the corresponding authors upon reasonable request.

Supplemental Document. See Supplement 1 for supporting content.

REFERENCES

1. A. Pikovsky, M. Rosenblum, and J. Kurths, "Synchronization of a periodic oscillator by external force," in *Synchronization: A Universal Concept in Nonlinear Sciences*, Cambridge Nonlinear Science Series (2003), Vol. **12**, p. 432.
2. A. Arenas, A. Díaz-Guilera, J. Kurths, Y. Moreno, and C. Zhou, "Synchronization in complex networks," Phys. Rep. **469**, 93–153 (2008).
3. E. Niebur, H. G. Schuster, D. M. Kammen, and C. Koch, "Oscillator-phase coupling for different two-dimensional network connectivities," Phys. Rev. A **44**, 6895–6904 (1991).
4. M. G. Rosenblum and A. S. Pikovsky, "Controlling synchronization in an ensemble of globally coupled oscillators," Phys. Rev. Lett. **92**, 1–4 (2004).
5. E. O. S. H. Strogatz, D. M. Abrams, A. McRobie, and B. Eckhardt, "Crowd synchrony on the millennium bridge," Nature **438**, 43–44 (2005).
6. P. Kolodner, S. Slimani, N. Aubry, and R. Lima, "Characterization of dispersive chaos and related states of binary-fluid convection," Phys. D **85**, 165–224 (1995).
7. D. Hansel, G. Mato, and C. Meunier, "Phase dynamics for weakly coupled Hodgkin-Huxley neurons," Europhys. Lett. **23**, 367 (1993).
8. T. Heil, I. Fischer, W. Elsässer, J. Mulet, and C. R. Mirasso, "Chaos synchronization and spontaneous symmetry-breaking in symmetrically delay-coupled semiconductor lasers," Phys. Rev. Lett. **86**, 795–798 (2001).
9. J. Ohtsubo, *Semiconductor Laser Networks: Stability, Instability and Chaos*, 4th ed., Springer Series in Optical Sciences (Springer, 2017), Chap. 14.
10. M. Nixon, E. Ronen, A. A. Friesem, and N. Davidson, "Observing geometric frustration with thousands of coupled lasers," Phys. Rev. Lett. **110**, 1–5 (2013).
11. Y. Shen, N. C. Harris, S. Skirlo, M. Prabhu, T. Baehr-Jones, M. Hochberg, X. Sun, S. Zhao, H. Larochelle, D. Englund, and M. Soljačić, "Deep learning with coherent nanophotonic circuits," Nat. Photonics **11**, 441–446 (2017).
12. D. Brunner, B. Penkovsky, B. A. Marquez, M. Jacquot, I. Fischer, and L. Larger, "Tutorial: Photonic neural networks in delay systems," J. Appl. Phys. **124**, 152004 (2018).
13. Q. Zhang, H. Yu, M. Barbiero, B. Wang, and M. Gu, "Artificial neural networks enabled by nanophotonics," Light Sci. Appl. **8**, 42 (2019).
14. J. R. Terry, K. S. Thornburg, D. J. DeShazer, G. D. VanWiggeren, S. Zhu, P. Ashwin, and R. Roy, "Synchronization of chaos in an array of three lasers," Phys. Rev. E **59**, 4036–4043 (1999).
15. R. Roy and K. S. Thornburg, "Experimental synchronization of chaotic lasers," Phys. Rev. Lett. **72**, 2009–2012 (1994).
16. M. Fridman, R. Pugatch, M. Nixon, A. A. Friesem, and N. Davidson, "Phase-locking-level statistics of coupled random fiber lasers," Phys. Rev. E **86**, 1–5 (2012).
17. Y. Liu, Y. Takiguchi, P. Davis, T. Aida, S. Saito, and J. M. Liu, "Experimental observation of complete chaos synchronization in semiconductor lasers," Appl. Phys. Lett. **80**, 4306–4308 (2002).
18. A. Argyris, M. Bourmpos, and D. Syvridis, "Experimental synchrony of semiconductor lasers in coupled networks," Opt. Express **24**, 5600–5614 (2016).
19. M. Montinaro, V. Resta, A. Camposeo, M. Moffa, G. Morello, L. Persano, K. Kazlauskas, S. Jursenas, A. Tomkeviciene, J. V. Grazulevicius, and D. Pisignano, "Diverse regimes of mode intensity correlation in nanofiber random lasers through nanoparticle doping," ACS Photonics **5**, 1026–1033 (2018).
20. M. Höfner, H.-J. Wünsche, and F. Henneberger, "A random laser as a dynamical network," New J. Phys. **16**, 033002 (2014).
21. M. Gaio, D. Saxena, J. Bertolotti, D. Pisignano, A. Camposeo, and R. Sapienza, "A nanophotonic laser on a graph," Nat. Commun. **10**, 1–7 (2019).
22. S. Krämmer, C. Vannahme, C. L. C. Smith, T. Grossmann, M. Jenne, S. Schierle, L. Jørgensen, I. S. Chronakis, A. Kristensen, and H. Kalt, "Random-cavity lasing from electrospun polymer fiber networks," Adv. Mater. **26**, 8096–8100 (2014).

23. H. Cao, Y. G. Zhao, H. C. Ong, S. T. Ho, J. Y. Dai, J. Y. Wu, and R. P. H. Chang, "Ultraviolet lasing in resonators formed by scattering in semiconductor polycrystalline films," Appl. Phys. Lett. **73**, 3656–3658 (1998).
24. D. S. Wiersma, P. Bartolini, A. Lagendijk, and R. Righini, "Localization of light in a disordered medium," Nature **390**, 671–673 (1997).
25. H. Cao, Y. G. Zhao, S. T. Ho, E. W. Seelig, Q. H. Wang, and R. P. H. Chang, "Random laser action in semiconductor powder," Phys. Rev. Lett. **82**, 2278–2281 (1999).
26. B. Redding, M. A. Choma, and H. Cao, "Speckle-free laser imaging using random laser illumination," Nat. Photonics **6**, 355–359 (2012).
27. A. Boschetti, A. Taschin, P. Bartolini, A. K. Tiwari, L. Pattelli, R. Torre, and D. S. Wiersma, "Spectral super-resolution spectroscopy using a random laser," Nat. Photonics **14**, 177–182 (2020).
28. K. Vynck, M. Burresi, F. Riboli, and D. S. Wiersma, "Photon management in two-dimensional disordered media," Nat. Mater. **11**, 1017–1022 (2012).
29. L. Cui, J. Shi, Y. Wang, R. Zheng, X. Chen, W. Gong, and D. Liu, "Retrieval of contaminated information using random lasers," Appl. Phys. Lett. **106**, 201101 (2015).
30. S. Biasco, H. E. Beere, D. A. Ritchie, L. Li, A. G. Davies, E. H. Linfield, and M. S. Vitiello, "Frequency-tunable continuous-wave random lasers at terahertz frequencies," Light Sci. Appl. **8**, 1–13 (2019).
31. E. Ignesti, F. Tommasi, L. Fini, F. Martelli, N. Azzali, and S. Cavalieri, "A new class of optical sensors: a random laser based device," Sci. Rep. **6**, 35225 (2016).
32. Y. Wang, Z. Duan, Z. Qiu, P. Zhang, J. Wu, A. Dingke, and T. Xiang, "Random lasing in human tissues embedded with organic dyes for cancer diagnosis," Sci. Rep. **7**, 1–7 (2017).
33. X. Jiang, H. Cao, Y. Ling, J. Y. Xu, and C. M. Soukoulis, "Mode repulsion and mode coupling in random lasers," Phys. Rev. B **67**, 1–4 (2003).
34. A. Consoli and C. López, "Decoupling gain and feedback in coherent random lasers: experiments and simulations," Sci. Rep. **5**, 16848 (2015).
35. A. Consoli, E. Soria, N. Caselli, and C. López, "Random lasing emission tailored by femtosecond and picosecond pulsed polymer ablation," Opt. Lett. **44**, 518–521 (2019).
36. A. Consoli, D. M. da Silva, N. U. Wetter, and C. López, "Large area resonant feedback random lasers based on dye-doped biopolymer films," Opt. Express **23**, 29954–29963 (2015).
37. A. Consoli and C. Lopez, "Emission regimes of random lasers with spatially localized feedback," Opt. Express **24**, 10912–10920 (2016).
38. A. J. Steckl, "DNA—a new material for photonics?" Nat. Photonics **1**, 3–5 (2007).
39. M. Leonetti, R. Sapienza, M. Ibisate, C. Conti, and C. López, "Optical gain in DNA-DCM for lasing in photonic materials," Opt. Lett. **34**, 3764–3766 (2009).
40. A. Consoli and C. López, "Lasing optical cavities based on macroscopic scattering elements," Sci. Rep. **7**, 40141 (2017).
41. L. N. G. Pearson and K. Filon, "Mathematical contributions to the theory of evolution. IV. On the probable errors of frequency constants and on the influence of random selection on variation and correlation," Philos. Trans. R. Soc. London A **101**, 229–311 (1898).
42. J. L. Rodgers and W. A. Nicewander, "Thirteen ways to look at the correlation coefficient," Am. Stat. **42**, 59–66 (1988).
43. R. De Gelder, R. Wehrens, and J. A. Hageman, "A generalized expression for the similarity of spectra: application to powder diffraction pattern classification," J. Comput. Chem. **22**, 273–289 (2001).
44. A. Kraskov, H. Stögbauer, and P. Grassberger, "Estimating mutual information," Phys. Rev. E **69**, 16 (2004).
45. H. A. Haus, "Mode-locking of lasers," IEEE J. Sel. Top. Quantum Electron. **6**, 1173–1185 (2000).
46. C. Conti, M. Leonetti, A. Fratalocchi, L. Angelani, and G. Ruocco, "Condensation in disordered lasers: theory, 3D+1 simulations, and experiments," Phys. Rev. Lett. **101**, 2–5 (2008).